tACS competes with ongoing oscillations for control of spike-timing in the primate brain

Matthew R. Krause[1,3,4], Pedro G. Vieira[1,3], Jean-Philippe Thivierge[2] and Christopher C. Pack[1*]

[1] Department of Neurology and Neurosurgery, Montreal Neurological Institute, McGill University, Montreal, Quebec, Canada
[2] School of Psychology, University of Ottawa, Ottawa, Ontario, Canada.
[3] These authors contributed equally.
[4] Lead contact
* Correspondence: christopher.pack@mcgill.ca

Summary

Transcranial alternating current stimulation (tACS) is a promising but controversial method for modulating neural activity noninvasively. Much of the controversy revolves around the question of whether tACS can generate electric fields that are strong enough to entrain neuronal spiking activity. Here we show that what matters is not the electric field strength per se, but rather the strength of the stimulation relative to ongoing oscillatory entrainment. We recorded from single neurons in the cortex and subcortex of behaving non-human primates, while applying tACS at different frequencies and amplitudes. When neuronal activity was weakly locked to ongoing oscillations, tACS readily entrained single-neuron activity to specific stimulation phases. In contrast, neurons that were strongly locked to ongoing oscillations usually exhibited decreased entrainment during low-amplitude tACS. As this reduced entrainment is a property of many oscillating systems, attempts to impose an external rhythm on spiking activity may often yield precisely the opposite effect.

Keywords: tES I tACS I transcranial alternating current stimulation I spike timing I oscillations I brain stimulation I asynchronous quenching

Introduction

Many aspects of brain function rely on rhythmic patterns of neural activity (Fries, 2015). Consequently, methods for altering spike timing are of interest, both as a research tool and as a potential intervention in certain disease states (e.g., Mogul and van Drongelen, 2014, Grover et al., 2021). Transcranial electrical stimulation (tES) is a family of such methods, which modulate brain activity by passing current through electrodes attached to the scalp. Compared to other neuromodulation techniques, tES has the advantages of being non-invasive, low-cost, and largely free of side effects. Transcranial alternating current stimulation (tACS), in which the current is modulated sinusoidally, has been of particular interest because its waveform resembles neural oscillations, which suggests that it may be able to modulate or control them.

During tES, currents applied to the scalp are generally low amplitude (2-4 mA) for safety and tolerability reasons, and much of it never even reaches the brain (Voroslakos et al., 2018). The electric fields produced within the brain are therefore relatively weak, on the order of 1 V/m or less. Nevertheless, there is strong evidence that these fields can entrain neural activity *in vitro* (Chan and Nicholson, 1986, Anastassiou et al., 2011), in small animal models, (Frohlich and McCormick, 2010, Ozen et al., 2010) and even in the large, well-insulated primate brain (Johnson et al., 2020, Krause et al., 2019).

Several mechanisms could produce this entrainment (Liu et al., 2018, Reato et al., 2013). Early work had suggested that tES provided enough input to completely elicit or suppress action potentials (Bindman et al., 1964). However, more recent biophysical modeling and direct measurements have found that the membrane potential polarization caused by tACS is insufficient to do so (Radman et al., 2009), which is confirmed by reports that average firing rates do not change during tACS (Johnson et al., 2020, Krause et al., 2019). Instead, tACS likely acts by producing sub-threshold fluctuations in neurons' membrane potentials that shift the timing of spikes (Reato et al., 2010, Deans et al., 2007). As a result, the externally-applied stimulation must interact in some way with the rhythms that are continually generated by a living brain (Herrmann et al., 2016).

The nature of these interactions is unclear. Some have suggested that the influence of tACS is so weak that it is overwhelmed by endogenous activity, especially when they are strong (Voroslakos et al., 2018, Berenyi et al., 2012). Other work argues that tACS act synergistically with ongoing oscillations, so as to enhance them (Feurra et al., 2013), but the mechanisms that might generate such synergy at the single-neuron level have not yet been identified. The latter hypothesis is the rationale for the vast majority of tACS studies, including hundreds of clinical trials. As a result, understanding precisely how tACS interacts with ongoing brain activity is essential for its effective use.

Here, we characterize the interaction between tACS and ongoing oscillations of varying strength, by recording single-neuron activity in the non-human primate brain. We confirm that tACS can strongly entrain neural activity, but we find that this phenomenon is limited to cases in which spike entrainment to ongoing activity is weak. Surprisingly, when neurons are strongly locked to ongoing activity, applying tACS often leads to a *decrease* in entrainment instead, which can only be reversed at higher stimulation amplitudes. These effects are accompanied by

changes in the oscillatory phase at which spikes are entrained. All these influences are well captured by a simple mathematical model of interacting oscillators.

Together, these results suggest that tACS competes with ongoing brain oscillations for control of spiking activity. Given the strength of ongoing oscillations in the behaving brain, the net result in human tACS use may often be a decrease in neural entrainment, which is precisely the opposite of the intended influence for many tACS studies. However, this reduced entrainment also explains some of the well-known behavioral effects of tACS. It also suggests new avenues for regulating neural synchrony with non-invasive brain stimulation.

Results

We examined the interplay of ongoing oscillations and tACS-generated entrainment, using recordings from non-human primates (*M. mulatta*), a model system that captures many aspects of human anatomy, physiology, and tACS use. Animals were trained to perform a simple visual fixation task that minimized sensory and cognitive factors which might influence oscillations. As animals performed this task, we recorded single-unit and local field potentials (LFPs), using standard neurophysiological techniques.

Our experiments targeted cortical area V4, where neurons often exhibit reliable entrainment to the local field potential (LFP) (Zanos et al., 2016, Zanos et al., 2015, Chalk et al., 2010, Bichot et al., 2005), especially in the 3-7 Hz "theta" frequency band (Spyropoulos et al., 2018). We verified that this occurred spontaneously in our data by computing phase-locking values (PLVs) that describe the consistency of spike timing (see *STAR Methods*). These values range from zero (spiking occurs randomly across an oscillation's cycle) to one (spiking occurs at only a single phase). Under our experimental conditions, many V4 neurons were locked to the 5 Hz component of the V4 LFP, but entrainment to higher frequency components, especially above 20 Hz, was minimal (Figure S1). The strength of entrainment at 5 Hz varied across neurons, from 0 to 0.42; such heterogeneity provides an ideal way to test interactions between tACS and the strength of entrainment to ongoing oscillations.

tACS can cause bidirectional changes in spike timing

Next, we recorded from the same V4 neurons during the application of tACS at an amplitude of ± 1 mA. Our stimulation methods closely mimicked those commonly used in human studies and produce an electric field of similar strength (~ 1 V/m). The effects of tACS were assessed by comparing PLVs obtained during blocks of tACS against those computed from intervals of baseline or "sham" stimulation that were randomly interleaved as a control.

Data from four example neurons are shown in Figure 1A, which summarizes the phases at which spikes occurred during the baseline (blue) and tACS (orange) conditions. For these cells, the entrainment to the ongoing oscillation was weak, and the application of tACS led to a significant increase in phase-locking ($p < 0.05$, per-cell randomization tests; see *STAR Methods*). These effects resemble those reported previously in other brain regions (Vieira et al., 2020, Krause et al., 2019, Johnson et al., 2020), but for the V4 population increased entrainment was found in only a small fraction (11%; N=17/157) of the neuronal population.

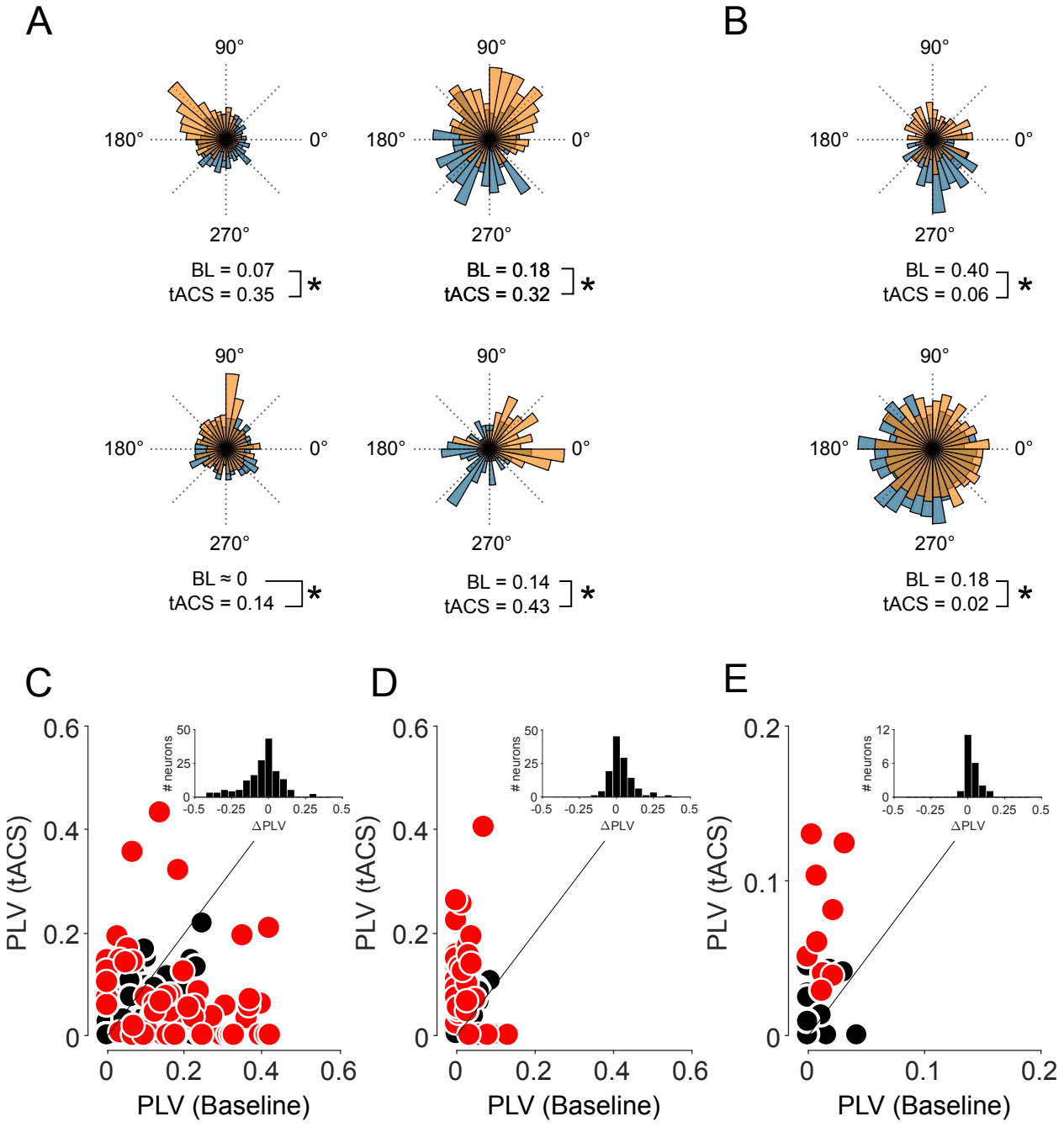

Figure 1. Applying tACS during physiological oscillations results in bidirectional changes in spike timing. **A–B)** Spike-density histograms for six example V4 neurons showing the relative amounts of spiking across an oscillatory cycle. The cells in (A) showed increased entrainment, while those in (B) have decreased entrainment during 5 Hz tACS (orange) compared to the baseline LFP (blue, BL). PLV values for each condition are shown below; asterisks indicate $p < 0.01$. **C–E)** Each point in the scatter plots represents a neuron's PLV during baseline (horizontal position) and tACS (vertical). Data were collected (C) in the presence of a 5 Hz ongoing oscillation within V4 (N=157), (D) also in V4, but at 20 Hz, where the oscillation is weaker (N=123), and (E) again at 5 Hz but in the hippocampus (N=21), which also lacks strong 5 Hz oscillations under our conditions. Neurons showing individually significant changes in phase-locking are denoted in red ($p < 0.05$; per-cell randomization tests). Inset histograms show the changes in PLV across the population. Panel C adapted from Krause et al., (2019). See also Figure S1 for comparison of entrainment during baseline conditions.

For other neurons, the application of tACS *decreased* phase-locking relative to baseline, as shown in the two example neurons of Figure 1B. For cells like these, the distribution of spike times was more uniform during tACS than during baseline. Such decreases in entrainment were statistically significant for 30% (47/157) of the cells in our sample ($p < 0.05$; per-cell randomization tests). Across the entire population of 157 V4 cells, decreased entrainment was the predominant influence of 5 Hz tACS, as the median PLV decreased from 0.066 (95% CI: [0.044--0.085]) to 0.031 [0.007--0.058], a statistically significant reduction in rhythmicity ($p < 0.01$; $Z = 3.86$; Wilcoxon sign-rank test).

The decreased entrainment neurons in Figure 1B had higher levels of baseline entrainment than the tACS-entrained neurons in Figure 1A. This pattern was evident in our complete dataset, where baseline entrainment was significantly and negatively correlated with the subsequent change in entrainment during tACS ($\rho = -0.38$; $p < 0.01$). This correlation persisted even after the application of Oldham's method (Oldham, 1962) to guard against regression to the mean; a permutation-based analysis (Kar et al., 2017) yielded similar results.

These effects were confined to a narrow window around the stimulation frequencies. An analysis of PLV values calculated in ±1 Hz bands from 2-100 Hz revealed significantly increased entrainment only in the 2-7 Hz. Likewise, cells that showed decreased entrainment did not, on average, become coupled to any other frequency component during stimulation (all $p > 0.05$; Wilcoxon sign-rank tests). As in previous studies, firing rates were not significantly different ($p > 0.1$; $Z = 1.63$; Wilcoxon sign-rank) between baseline (4.6 [3.7—5.8] Hz) and tACS (3.9 [3.4 – 5.4] Hz). This suggests that changes in entrainment were not due to a loss of single-unit isolation during tACS. Other technical controls, using the same recording apparatus, are described in *STAR Methods* and (Krause et al., 2019).

Decreased entrainment is not caused by choice of stimulation frequency or brain region

The decreased entrainment we have observed may seem at odds with results from previous studies, which have consistently reported increased entrainment with tACS, for spikes recorded from different brain regions and with different tACS frequencies (Vieira et al., 2020, Krause et al., 2019, Johnson et al., 2020, Ozen et al., 2010, Frohlich and McCormick, 2010). We therefore asked whether the lack of entrainment was due to our choice of brain region or stimulation frequency.

As a within-area control, we applied tACS to V4 at 20 Hz instead. For this frequency, baseline entrainment for V4 neurons was typically very weak (median: 0.01; 95% CI: [0 – 0.018]), with only 1/123 neurons having a PLV above 0.1. Against this low level of baseline entrainment, 20 Hz tACS caused 22 percent (27/123) of neurons to fire significantly more rhythmically ($p < 0.05$; per-cell randomization test; Figure 1B). The population PLV was significantly increased ($p < 0.01$, $Z = -3.945$; Wilcoxon sign-rank test), rising to 0.029 [0 – 0.050]. These data demonstrate that V4 neurons can be entrained by tACS at a different frequency.

As a within-frequency control, we also examined neural entrainment in the hippocampus, where baseline entrainment at 5 Hz was also weak. The median PLV was 0.01 and none of the 21 cells in our sample exhibited a PLV above 0.1. During 5 Hz tACS, entrainment increased in 9 of 21 hippocampal neurons (42%), and the median PLV significantly increased from 0.0083 [0 – 0.02] to 0.04 [0.01 – 0.05] ($p < 0.01$; $Z=-3.06$; Wilcoxon sign-rank test; Figure

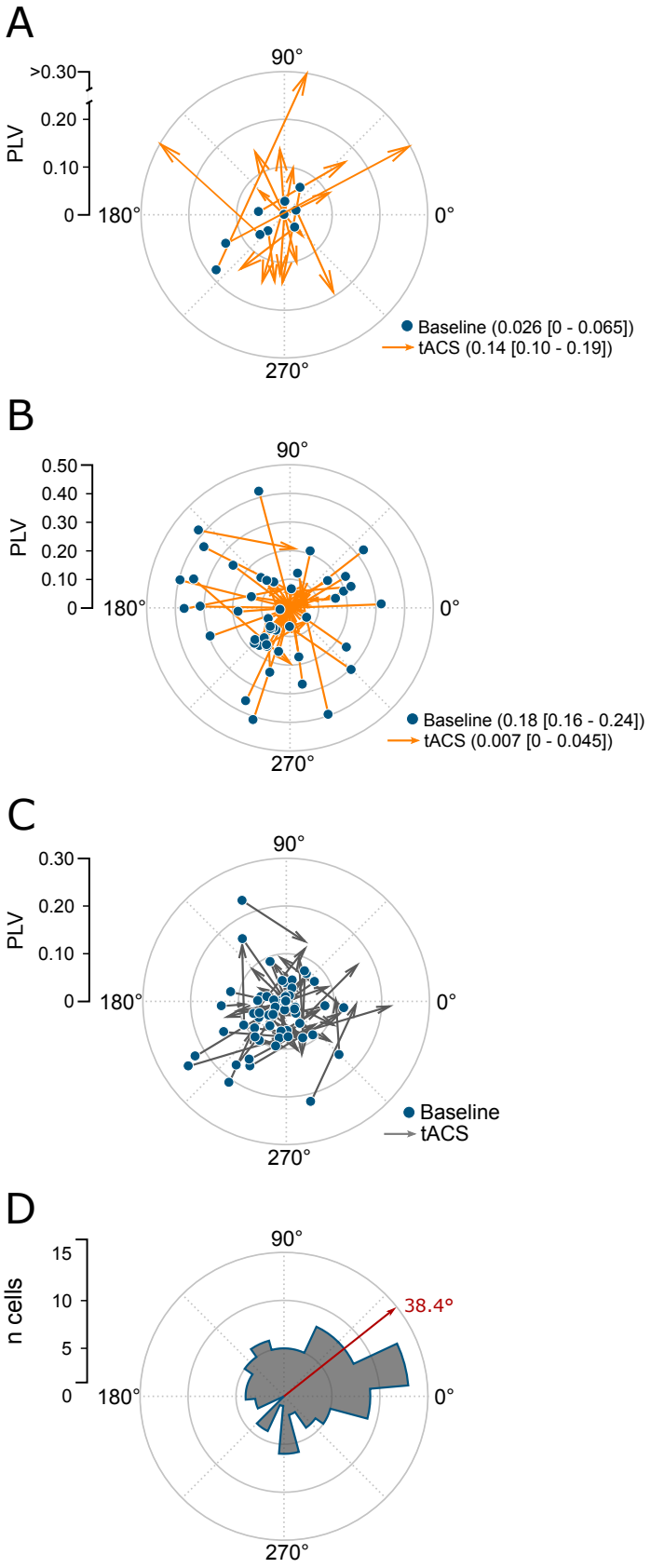

1C). Together, these results show that decreased entrainment is not necessarily a feature of V4 neurons nor of 5Hz tACS, both of which can be associated with increased entrainment under the right circumstances.

tACS alters the strength and phase of entrainment

Competition between an ongoing oscillation and the tACS waveform for control of spiking could explain these results (Liu et al., 2018, Chander et al., 2016). Specifically, we hypothesized that when baseline entrainment is weak, tACS can directly entrain neurons to its own waveform. However, when it is stronger, tACS may need to overcome the entrainment to the ongoing oscillation before imposing its own rhythm on the spikes. While the PLV measure used above captures the overall rhythmicity of spiking across tACS cycles, such a competition should also affect the timing of spikes *within* a tACS cycle. This aspect is captured by

Figure 2. Ongoing oscillations determine the strength and phase of tACS entrainment.
A–C) Polar plots summarizing the combined effects of tACS on entrainment strength (PLV, eccentric direction) and entrainment phase (polar angle). Each vector begins during baseline (BL; blue dot) and extends to 1 mA tACS (arrowhead). Vectors are grouped based on the change in PLV: (A) significant increase in PLV (individual $p < 0.05$; N=17), (B) significant decrease in PLV (individual $p < 0.05$; N=47) and (C) No significant change in PLV (N=93). **D)** Polar histogram showing the change in preferred phase for the neurons in Panel C. This is equivalent to the direction of the arrows shown in Panel C. The red arrow indicates the mean direction, 38.4°.

the neuron's preferred phase of spiking.

Figure 2 plots the PLVs and preferred phases jointly for each neuron. The radial distance from the origin of each plot corresponds to a neuron's PLV, while the angular position denotes the phase preference. Vectors connecting the baseline values (blue dots) with those measured during tACS (arrow tips) therefore completely describe the effects of stimulation on spike timing. Cells that show significantly increased entrainment during tACS tend to head outwards from the origin towards the oscillation's extrema (Figure 2A). The significantly desynchronized neurons, which by definition began with a pre-existing phase preference, start from locations uniformly distributed around the circle ($p = 0.092$; $\kappa = 0.72$ Hodges-Ajne omnibus test) and head inwards (Figure 2B). Thus, tACS tends not to reinforce or combine with existing phase preferences.

Instead, tACS appears to cause a shift in the preferred phase. For some cells, such as the two example neurons in right column of Figure 1A, this shift occurred in tandem with an increase in PLV. Interestingly, we also observed the same phenomenon even in neurons for which the overall PLV did not significantly change (Figure 2C). Rather, the primary effect of tACS on these cells appeared to be a rotation in the phase of entrainment.

Note that, for both the baseline and tACS conditions, our estimates of oscillation phase were defined relative to the electric potential within the extracellular space near each neuron. For the baseline condition, this reflects the LFP, while for the tACS condition it is dominated by the instantaneous phase of tACS, as detected by our recording electrode. Thus, the observed differences in the preferred phase of spiking cannot be attributed to a difference in referencing conditions (Shirhatti et al., 2016), as these were identical in both conditions. Monitoring the tACS waveform near our recording site also accounted for any phase distortion caused by the passage of current through the head (Noury et al., 2016).

Moreover, the change in phase observed with tACS cannot be attributed simply to phase differences between tACS and ongoing oscillations. Given the open-loop nature of our experiments, this difference was random from block to block, but the change in phase between baseline and tACS conditions exhibited a highly consistent preference of approximately 38˚($p < 0.001$; Hodges-Ajne omnibus test; Figure 2D). We therefore suggest that these phase shifts reflect a combination of the effects shown in Figures 2A and 2B, where tACS first decouples neurons from their entrainment to the ongoing oscillation, and then resynchronizes to the stimulation waveform at a new phase.

tACS desynchronizes, then re-entrains neural activity

To test this possibility, we collected additional data from 47 V4 neurons, using both the original ±1 mA stimulation, as well as ±2 mA. We reasoned that if weak stimulation were partially reducing entrainment to a physiological oscillation, stronger electric fields could completely overcome it and lead to increased entrainment to the tACS waveform (Park et al., 2005). Figure 3 shows the results of this experiment as a series of points on a polar vector field. As in Figure 2, the location of each blue dot represents a neuron's baseline entrainment, in terms of overall PLV (radial distance from the origin) and preferred phase (angle). Spike timing during ±1 mA is depicted by orange dots, and ±2 mA by red dots. The lines joining them create a vector that shows the effects of increasing current on spike timing.

For many neurons, applying ±1 mA tACS decreased or eliminated entrainment relative to baseline, but the stronger ±2 mA stimulation reinstated some entrainment, often at a different phase. The example neuron shown in Figure 3A had a PLV of 0.159 under baseline conditions, no detectable entrainment during ±1 mA tACS (PLV ≈ 0), and a PLV that again reached 0.158 during ± 2 mA stimulation. During this transition from 0 to ±2 mA stimulation, its preferred phase rotated from 191˚to 83˚. While a naïve analysis that considered only changes in PLV might conclude that this neuron was insensitive to tACS, these data demonstrate that the structure of its spike timing is, in fact, altered by the stimulation.

Other neurons progressively lost entrainment as the stimulation amplitude increased. This pattern appears in the example cell shown in Figure 3B, whose PLVs decreased from 0.21 to 0.092, to nearly 0 as the tACS amplitude increased, with the phase consistently remaining near

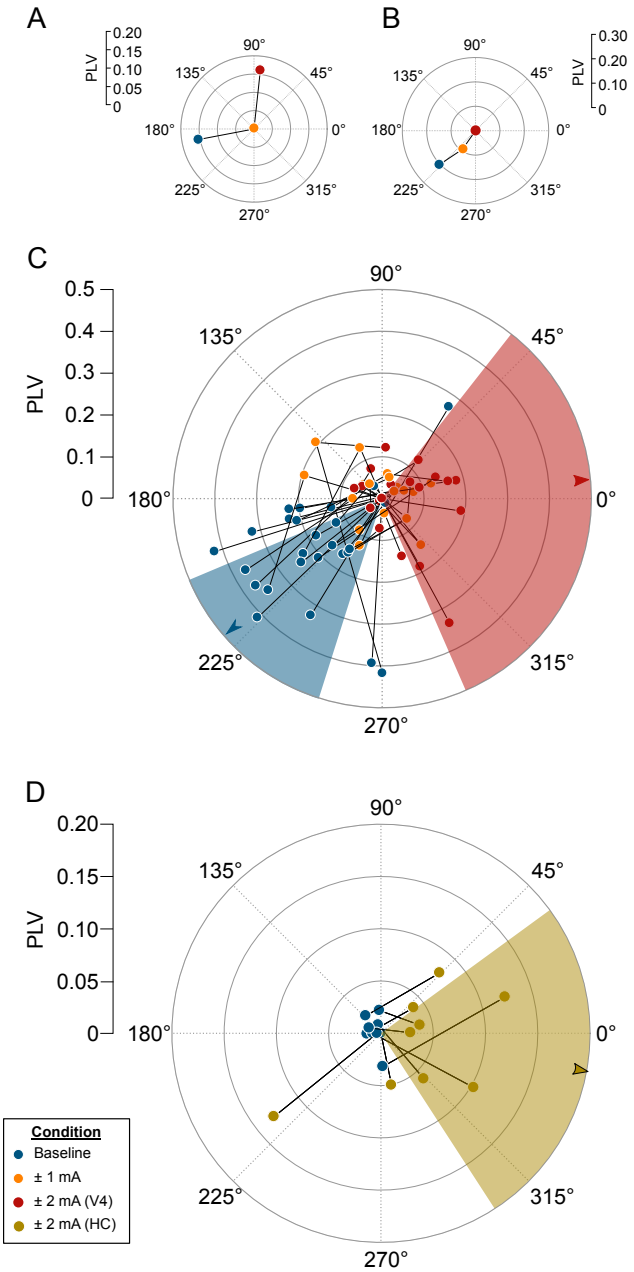

Figure 3. tACS reduces entrainment, then reinstates it at a different phase, as the stimulation amplitude increases. A-C) Polar vectors indicating the phase and strength of V4 neurons' entrainment (as in Figure 3. The blue dots indicate baseline conditions (blue), followed by ±1 mA tACS (orange) and ±2 mA tACS (red). Shading indicates the median and 95% confidence interval of the phase preference during baseline (blue) and ±2 mA tACS (red). Panels A and B show an example trajectory for one neuron exhibiting reinstated entrainment (A) and another undergoing progressive decreases in entrainment (B). Panel C shows population data from 27 neurons with significant changes in PLV at either amplitude. **D)** Data from N=9 hippocampal neurons during baseline (blue dot) and ±2 mA tACS (olive), plotted as in Panel A. Note that ±2 mA tACS produces an electrical field within the hippocampus that is three times weaker than the ±1 mA condition for V4.

225˚(223˚, 235˚, and 221˚, respectively). These patterns are common in our data, as shown in Figure 3C, which depicts the trajectories through 0, ±1, and ±2 mA for the 27/47 neurons (57%) in our data set that showed significant changes from their baseline PLV at either tACS intensity. Thus, it appears that changes in preferred phase emerge only after spiking has been fully decoupled from the ongoing oscillation.

We present a similar diagram for our hippocampal data in Figure 3D. Although the electric field reaching this deep structure was far weaker (0.2—0.3 V/m; Krause et al., 2019), nearly half of these neurons (9/21; Figure 1C) showed increased entrainment, reminiscent of the ±2 mA condition in V4. Critically, these neurons' baseline levels of entrainment were near zero, so it was not necessary to overcome any substantial baseline entrainment. Nevertheless, the preferred phase for these neurons was similar to that observed in V4 (Figure 3C). Overall, these results, across stimulation frequencies, stimulation amplitudes, and brain regions, show consistently that tACS influences spiking activity in a manner that depends strongly on the levels of pre-existing entrainment.

Similar patterns of effects emerge from a simple oscillator model

Our experimental results show a specific pattern of reduced entrainment from baseline, followed by restored entrainment at higher stimulation amplitudes. Although there are many ways in which tACS can interact with ongoing oscillations (reviewed in Reato et al., 2013), most previous experimental work has not reported decreased entrainment. We therefore sought to determine whether decreased entrainment has a theoretical basis in the properties of coupled oscillators. Specifically, we explored the properties of a simple oscillator model that consists of two equations (Doelling and Assaneo, 2021):

$$\frac{dx}{dt} = \lambda x - \omega y - \gamma\left(x^2 + y^2\right)x + ks(t)$$
$$\frac{dy}{dt} = \lambda y + \omega y - \gamma\left(x^2 + y^2\right)y$$

Here, x and y represent the dynamics of two coupled populations of neurons, whose interactions generate an oscillation. For simplicity, we assumed that higher amplitude oscillations were associated with stronger phase-locking, as found in previous experimental work (Deans et al., 2007, Ozen et al., 2010).

We simulated the effects of tACS by changing the properties of the external drive *s(t)*. As in our experiments, *s(t)* was either zero (for baseline conditions) or a sine wave of given frequency and phase offset for the tACS condition. The coupling parameter k determines how strongly this external drive affects the neuronal population. In the results below, we express k as a percentage of the ongoing oscillation's amplitude, which simplifies the model.

We first asked whether a consistent phase offset between an ongoing oscillation and tACS at the same frequency could account for our results. It did not. Stimulation applied at all *phase* offsets led to phase shifts in the ongoing oscillation, accompanied by an increase in its amplitude. For example, Figure 4A shows that applying even 180˚out-of-phase stimulation of 5%, 30%, and 75% increased the oscillation's amplitude by 5%, 26%, and 49% respectively, while shifting the phase by up to a quarter cycle relative to the no-stimulation condition.

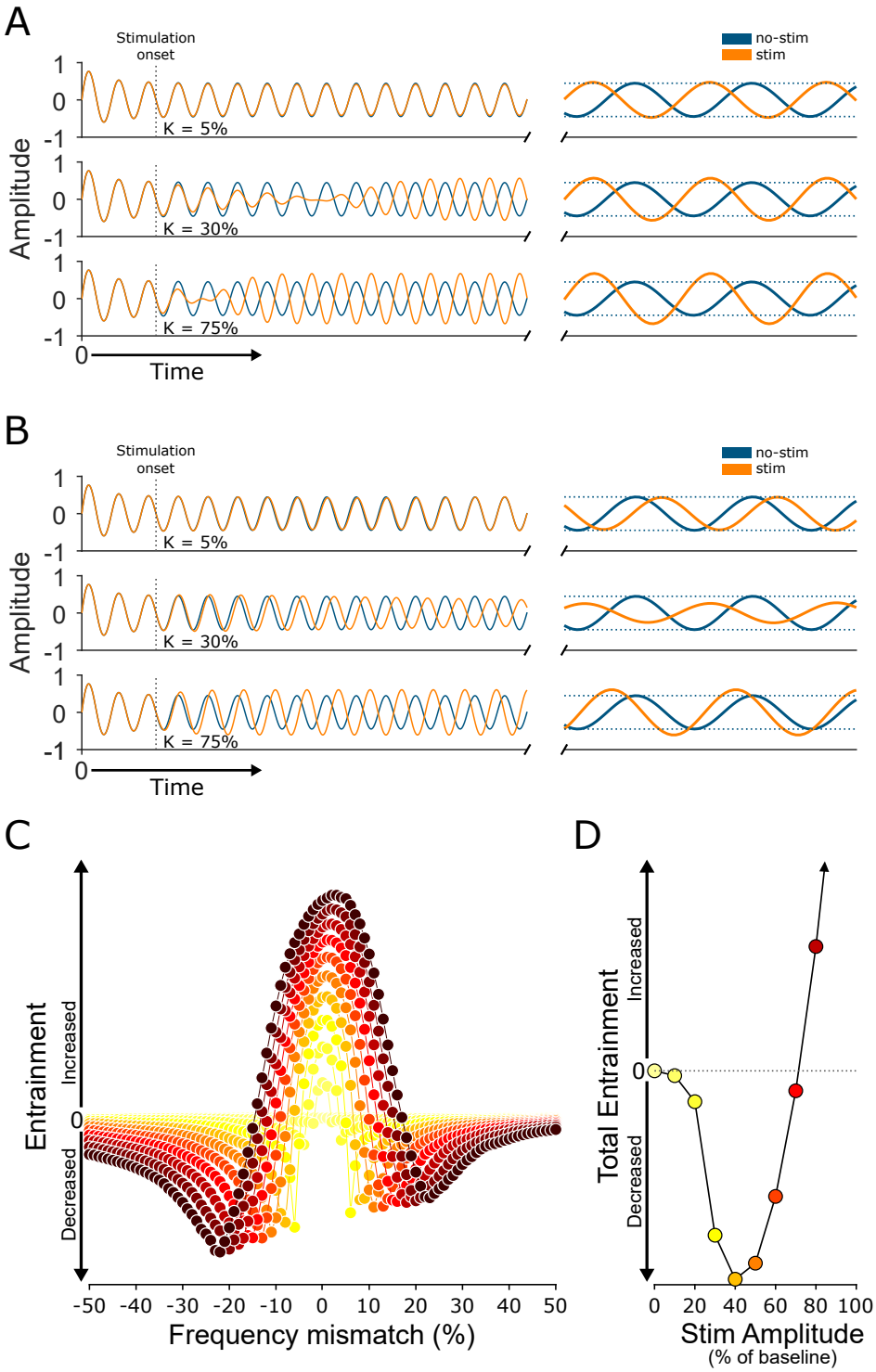

Figure 4. A simple oscillator model replicates these results A) Stimulating the Stuart-Landau model at the same frequency tends to increase entrainment and shift phase. The model's output, *x(t)*, is shown during a no-stimulation condition (blue) and during the application of tACS (yellow) at low (top), medium (middle), and high (bottom) stimulation intensities. The other component of the model, *y(t)*, is simply a phase-shifted version of *x(t)* and shows the same pattern of effects, as shown in Figure S2. **B)** Stimulation applied at a slightly different frequency tends to reduce entrainment instead. The model output is plotted as in Panel A. **C)** Changes in entrainment, as a function of frequency mismatch and stimulation intensity. **D)** Changes in total entrainment, calculated by integrating the curves in Panel C. Colors correspond to those used in Panel C.

We next asked whether slight differences between the *frequencies* of tACS and the ongoing oscillation could account for our results. This did seem to be the case: Figure 4B shows that applying stimulation at frequency that was only 6% below that of the ongoing oscillation led to an 29% decrease in amplitude at moderate stimulation intensities (k=30%; middle row of Figure 4B), followed by a 35% increase at higher intensities (k=75%; bottom row of Figure 4B). Stimulation that was instead slightly higher in frequency had similar effects, causing a 25% decrease, followed by a 44% increase (not shown) in the ongoing oscillation's amplitude. Importantly, this effect on the strength of entrainment was independent of the relative phases of the tACS and ongoing oscillations. Figure 4C summarizes this effect for a range of relative frequencies, by averaging across relative phases, for consistency with the open-loop nature of our experiments. Stimulation that precisely matched the oscillation's frequency led to increased oscillation strength, but detuning the frequency by even a fraction of a cycle reduced the amplitude noticeably when the stimulation amplitude was relatively weak.

In real experiments, such a mismatch is likely unavoidable, given variability in spike timing (Softky and Koch, 1993) and peak frequencies within an oscillation (Mansouri et al., 2017), as well as the non-sinusoidal nature of neural oscillations (Burns et al., 2011, Cole and Voytek, 2017). We therefore integrated the curves of Figure 4C across frequencies for each stimulation intensity to mimic the drift in these parameters (Figure 4D). Initially, the total entrainment within a narrow frequency band decreased, but when the stimulation amplitude exceeded about 66 percent of the on-going oscillation's amplitude, entrainment increased. Measurements of ongoing membrane potentials (Schaefer et al., 2006, Bilkey and Heinemann, 1999) indicate that they are often several times larger than polarization produced by tACS (Radman et al., 2009), so tACS, as applied in human experiments, may often lie near this transition.

Baseline frequency preference determines the effects of tACS

A straightforward prediction of this model is that entrainment should be most strongly reduced for neurons with frequency preferences that are displaced from the stimulation frequency (i.e., in the flank of the entrainment vs. frequency-mismatch curve in Figure 4C). To test this prediction, we reanalyzed our V4 data to identify each neuron's baseline frequency preference with greater precision (in ±0.25 Hz frequency bands from 2-8 Hz). We calculated the PLV within each bin of these narrowband signals and assigned the bin with the highest baseline PLV as the neuron's preferred narrowband frequency (Figure 5A).

Figure 5B shows that, of the 47 neurons showing significantly decreased entrainment during 5 Hz tACS, most had baseline frequency preferences 1-2 Hz away from the stimulation frequency, reminiscent of the flank of Figure 4C. Only one neuron with decreased entrainment had a baseline frequency preference between 4.75–5.25 Hz. Owing to their low baseline entrainment, no pre-existing frequency preference could be identified for the 17 neurons that exhibited increased entrainment during tACS. These results demonstrate a strong but qualitative agreement with models of competing oscillators.

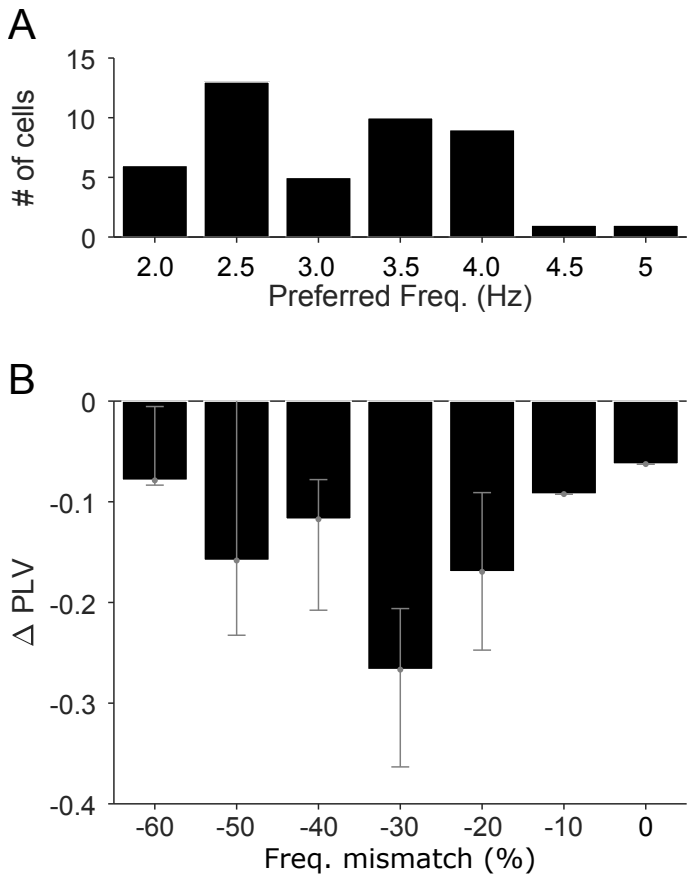

Figure 5. Pre-existing frequency preference determines the effects of tACS. A) Histogram of narrowband preferred frequency for the 47 V4 neurons with significantly decreased entrainment during 5 Hz tACS. **B)** Changes in these neurons' PLV as a function of the difference between their narrowband preferred frequency and the 5 Hz tACS frequency. Note the qualitative similarity to the flank of Figure 4C.

Excitatory and inhibitory cells are similarly affected by tACS

The model makes another specific prediction that is of immediate biological relevance. Previous work has suggested that tACS may preferentially target certain types of neurons: due to their morphology, interneurons have been proposed to be less susceptible to tACS (Aberra et al., 2018, Radman et al., 2009), while due to their positions with neural circuits, others have suggested they are more strongly affected by it (Huang et al., 2021). In the model, stimulation is applied to one subpopulation (the *x* term above), but both subpopulations are affected similarly by the stimulation (Figure S2), due to the tight coupling between them. This suggests that all neurons, regardless of cell type, will be affected similarly by tACS.

We therefore asked whether cell type could explain the mix of increased and decreased entrainment shown in Figure 1C. Putative cell types were identified via their spike widths: narrow-spiking neurons are often interneurons, while those with broader spikes are more likely to be pyramidal cells (See *STAR Methods* and Figure 6A). As predicted from the model, broad-spiking neurons were no more likely than narrow-spiking neurons to be significantly modulated, in either direction, by tACS ($p = 0.44$; $X^2(1) = 0.59$). When considering only the neurons affected by tACS (Figure 6B, colored dots), the two cell types did exhibit significantly different directions of modulation ($p < 0.01$; $X^2(1) = 12.1$). Entrainment overwhelmingly decreased in broad-spiking neurons (88%; 36/41 cells), but the effects on narrow-spiking neurons were more mixed: 12 of 23 narrow-spiking cells became more entrained during 5 Hz tACS, while 11 of 23 showed significantly reduced entrainment. However, this appears to be driven by differences in baseline

levels of entrainment: broad-spiking neurons tended to be strongly entrained at baseline, while narrow-spiking neurons fell into a weakly-entrained cluster with PLVs near 0 and a more strongly entrained one around 0.3 under baseline conditions. As in the full dataset, the effect of tACS on these narrow-spiking neurons was inversely correlated with baseline entrainment levels (Spearman's ρ = -0.38; p=0.083). Data collected during 20 Hz tACS, where both cell types showed minimal baseline entrainment, and subsequently became strongly entrained by 20 Hz tACS (Figure 6C), further supports this hypothesis. Thus, the effects of tACS appear largely determined by a cell's baseline level of entrainment, rather than cell type.

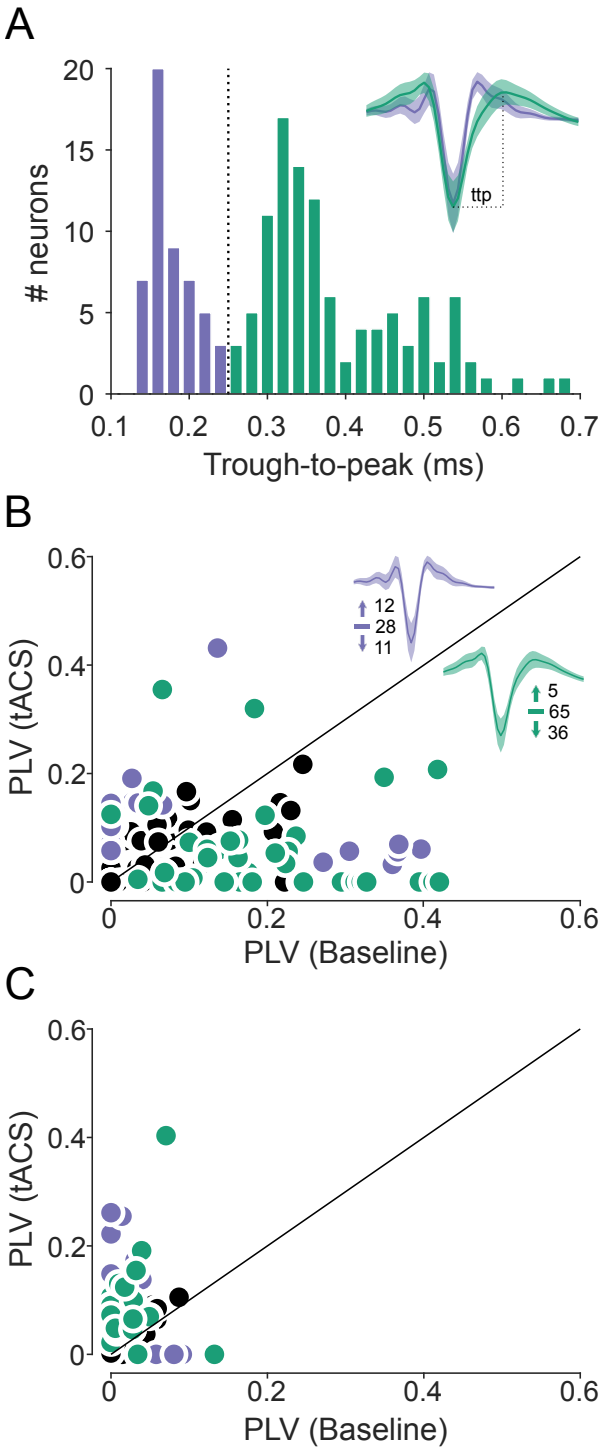

Figure 6. Distinct cell types are associated with tACS synchronization vs. desynchronization. A) Neurons (N=157) were divided using a trough-to-peak width threshold of 250 µs (dashed line). Narrow-spiking putative interneurons are shown in purple; broad-spiking pyramidal cells in green. Average waveforms for each class are inset. **B)** Changes in V4 neurons' spike timing during 5 Hz tACS, color-coded by cell type; neurons without significant changes in PLV are shown in black. Numbers near the waveforms indicate the number of cells showing significantly increased, unchanged, and decreased PLVs. The style is otherwise identical to Figure 1A. **C)** Changes in V4 neurons' spike timing during 20 Hz tACS (N=123), plotted as in Panel B.

Discussion

The results shown here demonstrate that tACS can produce bidirectional effects on the spike timing of individual neurons, causing them to fire either more or less rhythmically (Figure 1). The direction of these effects depends both on the relative strengths of entrainment to the ongoing physiological oscillation and the tACS-induced electric field (Figures 2 and 3). These data are consistent with a simple model (Figure 4) in which tACS competes with ongoing oscillations for control of spike timing, a hypothesis supported by several ancillary tests of the model (Figures 5 and 6).

Implications for clinical applications

The ability to bidirectionally modulate neuronal entrainment opens up a number of new therapeutic possibilities. Excess synchrony has been implicated in a wide range of conditions, including movement disorders, epilepsy, and schizophrenia (Venables et al., 2009), and stimulation that reduces it may provide a means for controlling these symptoms. Deep Brain Stimulation (DBS) has become a standard, albeit invasive and expensive, method for treating severe cases of some of these diseases. While the mechanisms of action are not completely understood, it seems increasingly likely that DBS acts by regulating spike timing in ways that reinstate normal patterns of activity, rather than merely suppressing pathologically strong amounts of activity (Santaniello et al., 2015). Our data suggests that tACS may be capable of producing similar effects non-invasively. Moreover, this may be quite easy to do.

Closed-loop systems, which sense an oscillation and then apply counter-phased stimulation to cancel it, have been proposed as a mechanism for controlling pathological neural activity (Mogul and van Drongelen, 2014, Holt et al., 2019). These relatively complicated systems may not always be necessary: weak, open-loop stimulation at a nearby frequency may suffice to reduce some oscillations. Under the names “asynchronous quenching” or “amplitude death”, this strategy has been used to control oscillations in contexts such as power and aeronautical engineering (Guan et al., 2019). Indeed, these phenomena are universal properties of self-excited, forced oscillators, such as the brain (Premraj et al., 2021).

At the same time, these data suggest that it may be much harder than expected to non-invasively increase neuronal entrainment to ongoing oscillations. To do so, stimulation must target brain regions and behavioral conditions in which ongoing entrainment is relatively weak, or else it must be precisely matched to both the frequency and phase of the on-going oscillation. The latter approach is challenging, because estimates of frequency and phase provide only transient approximations to the actual oscillations (Cole and Voytek, 2017), which drift on sub-second timescales (Mansouri et al., 2017, Burns et al., 2011). Thus, closed-loop stimulation may prove to be more useful for reinforcing existing oscillations (Ketz et al., 2018). However, most human tACS use is currently performed open-loop, using waveforms of a fixed frequency. Since those experiments typically seek to “increase”, “enhance”, (e.g., Marchesotti et al., 2020) or “rescue” (e.g., Grover et al., 2021) an existing neural oscillation, our data raise the worrying possibility that many human tACS experiments have inadvertently produced the exact opposite of their intended effects.

Implications for behavioral studies

In that light, we suggest some alternative interpretations of well-established tACS behavioral effects. Detection of faint auditory (Wilsch et al., 2018), visual (Helfrich et al., 2014), and somatosensory (Gundlach et al., 2016) stimuli can often be improved by tACS (reviewed in Cabral-Calderin and Wilke, 2020). These results are often ascribed to synchronization between the sensory input and the tACS waveform, as would be expected if tACS further entrained neurons that were already locked to sensory input. However, our data demonstrate that tACS often decreases neural entrainment under these conditions. Interestingly, decreased neural synchrony can sometimes lead to improved sensory performance, as in perceptual decision-making (Liu et al., 2016, Zohary et al., 1994) or selective attention (Cohen and Maunsell, 2009). Some theories of attention propose that it improves visual performance by decreasing synchronization at lower frequencies, while simultaneously increasing it at higher ones (Fries et al., 2001). Since ongoing low-frequency oscillations tend to be strong, while entrainment to higher frequencies is often weak, a similar pattern of neural effects would seem to be an ideal way for tACS to improve performance on perceptual tasks. Similar mechanisms (Pasley et al., 2009, Allen et al., 2007) might account for improved sensory discrimination following transcranial magnetic stimulation, as suggested previously (Waterston and Pack, 2010).

More generally, our results suggest that the effects of tACS likely depend on the behavioral task, insofar as many tasks modulate the strength of ongoing neural oscillations. The 8–12 Hz "alpha" frequency band is a very common target of tACS, but endogenous alpha oscillations vary in amplitude, depending on task demands (Okuhata et al., 2013, Jensen et al., 2002) and the overall alertness of the subject (Klimesch, 2012). Moreover, the dominant frequency within the alpha band varies across subjects, in a manner that is correlated with age and sex (Chiang et al., 2011), clinical status (e.g., Mathewson et al., 2012), and other factors. As a result, the effects of fixed-frequency tACS (e.g., at 10 Hz) may vary across subjects as well as within a single subject as their performance of a task changes. Mechanisms like these may account for some of the extensive intra- and inter-subject variability observed in many tACS experiments (Kasten et al., 2019).

Previous neurophysiological studies, including our own, have not found correlations between baseline activity and tACS's effects. We suggest that this is due to Simpson's Paradox: the limited range of baseline PLVs in those studies masked the correlations reported here. However, our current findings are consistent with human tES experiments reporting similarly complex non-monotonic dose-response relationships on behavior (e.g., Ehrhardt et al., 2021). Our modelling suggests that conditions within the human brain are often near the "elbow" of the curve shown in Figure 4D and that it may be advantageous to try multiple stimulation intensities. Although considerable effort has been devoted to maximizing the field strength produced by tACS montages, future studies should consider the possibility that, for some goals, more, in terms of current or electric field strength, may not always be better.

Implications for biophysics

These data challenge previous work suggesting that tACS preferentially engages specific cell types. Based on their elongated, asymmetric morphology, pyramidal cells were predicted to be strongly susceptible to external electric fields while the smaller and bushier interneurons would

be much less affected (Radman et al., 2009, Aberra et al., 2018). Although these biophysical predictions are likely valid for isolated neurons, they are less relevant when the neurons are embedded in the complex, interacting networks of a living brain. Other work has suggested that network interactions cause tACS to produce especially strong effects in interneurons, which in turn drive the remaining neurons (Huang et al., 2021). This pattern is not evident in our data (Figure 6), where cells' ongoing patterns of activity, rather than morphology or identity, determine how they are affected by tACS. We note that these patterns of activity vary across cell types, brain areas, and behavioral states.

Conclusion

In summary, we have shown that the effects of tACS on individual neurons are determined by the interplay between ongoing oscillatory activity and the tACS waveform, with the differences in strength and frequency determining whether applying tACS results in more or less rhythmic spike timing. Producing predictable changes in neural activity, and ultimately, behavior, requires detailed knowledge of the relevant oscillations within the targeted brain areas. Our limited understanding of these phenomena, even in the absence of stimulation, may be an under-appreciated obstacle to using tACS. However, once these factors are understood and the stimulation tailored appropriately, the ability to increase and decrease the regularity of spike timing has numerous applications in the laboratory, clinic, and real world.

Acknowledgements

We thank Julie Coursol, Cathy Hunt, and Dr. Fernando Chaurand for outstanding technical assistance. This work was supported by Canadian Institutes of Health Research Grant MOP-115178 to CCP, and Parkinson's Canada Pilot Project Grant PPG-2020-0000000033 to MRK. The funders had no role in study design, data collection, analysis, decision to publish, or preparation of the manuscript.

Author Contributions

M.R.K., P.G.V. and C.C.P. designed research; M.R.K., and P.G.V., performed research; M.R.K. and P.G.V. analyzed the data; M.R.K., P.G.V., J.P.T., and C.C.P. performed formal analysis; M.R.K., P.G.V., J.P.T., and C.C.P. wrote the original manuscript and approved the final draft.

Declarations of Interest

The authors declare no competing interests.

STAR Methods

Resource Availability

Further information and requests for resources and reagents should be directed to and will be fulfilled by the lead contact, Matthew R. Krause (matthew.krause@mcgill.ca)

Materials Availability

This study did not generate new unique reagents.

Code and Data Availability

Preprocessed data and model code are data have been deposited at https://osf.io/9t2yp/?view_only=f678fff106274d67aaa65cbb36bf5c75 and are publicly available as of the date of publication. DOIs are listed in the key resources table. Owing to its large size, the raw electrophysiological data will be shared by the lead contact upon request. Any additional information required to reanalyze the data reported in this paper is available from the lead contact upon request.

Experimental Model and Subject Details

The results presented here are based on data collected from two adult male rhesus monkeys (*M. mulatta,* 7 and 10 years old; 8 and 14 kg, respectively). The complete dataset includes a reanalysis of the experiments described in Vieira et al. (2020) and Krause et al. (2019) as well as new data from 157 neurons that have not been reported previously. These new data were collected using approaches and techniques that were virtually identical to our previous work, which are described in detail below. All procedures were approved by the Montreal Neurological Institute's Animal Care Committee (Protocol #5031). The work was supervised by qualified veterinary staff, and followed the guidelines recommended by the Canadian Council on Animal Care. Animals received regular environmental enrichment, including access to a large play arena, and were socially housed when not in the laboratory. Animals were not assigned to specific experimental groups because the relevant unit of analysis are individual neurons, which were tested using a within-subject design (i.e., tACS vs baseline).

Behavioral Task

We used a simple fixation task to ensure that animals remained in a consistent behavioral state throughout the experiment. Animals sat in a standard primate chair (Crist Instruments, Hagerstown Maryland), placed 57 cm from a computer monitor that covered the central 30˚x 60˚ of the visual field. Eye position was monitored with an infrared eye tracker (SR Research, Ontario). The monkeys were trained to fixate a small black target (0.5˚) presented against a neutral grey background (54 cd/m^2) in exchange for juice rewards. Rewards were dispensed according to a schedule with a flat hazard function (exponential distribution with a mean of ~1 s). This arrangement minimized external factors known to influence oscillations, such as patterned visual stimulation, eye movements, and predictable rewards, allowing us to examine

the effects of tACS against a consistent background. Custom software written in Matlab (The Mathworks, Natick, MA, USA) controlled the behavioral task and coordinated the eye tracker, tES stimulator, and recording hardware.

Transcranial alternating current stimulation

We applied tACS in a manner designed to closely mimic human use. To plan the stimulation, individualized finite-element models were built from preoperative MRIs of each animal's head and neck (Datta, 2016). These were solved to identify electrode configurations that optimally stimulated neurons at our V4 and hippocampal recording sites. The hippocampal configurations produced an average field strength of 0.2 V/m (max: 0.35 V/m) in the hippocampus during ± 2 mA stimulation (Krause et al., 2019). Since V4 is on the cortical surface, the electric field therein was stronger: ~1 V/m at ±1 mA (Vieira et al., 2020). These conditions therefore bracket the best available estimates for field strengths achievable with two electrode-montages in humans. (Jackson et al., 2016, Huang et al., 2017). Our modelling approach also ensured that the brain implants required for these experiment do not produce abnormally strong electric fields elsewhere in the brain.

The stimulation was delivered through 1-cm "high-definition" Ag/AgCl electrodes (PISTIM; Neuroelectrics; Barcelona, Spain). These were coated with a conductive gel (SignaGel; Parker Laboratories, Fairchild New Jersey) and attached to the animals' intact scalps with a thin layer of Kwik-Sil (World Precision Instruments), a biocompatible silicon elastomer. Electrode impedance was typically between 1 and 2 kΩ, and always below 10 kΩ to prevent skin damage. In most experiments, current was applied via an unmodified StarStim8 system (Neuroelectrics, Barcelona, Spain). The stimulation waveform consisted of a 1.5- or 5-minute sinewave of the specified frequency (5 or 20 Hz) and amplitude (±1 or ±2 mA). At the beginning of each stimulation block, current was linearly ramped up from 0 to the maximum intensity over five seconds; this process was repeated in reverse at the end of each block. This minimizes the sensations produced by the onset and offset of stimulation. To measure baseline entrainment, "sham" stimulation repeated the initial and final ramps, without delivering current during the middle of the block. In a few sessions, a DC-STIMULATOR PLUS (NeuroConn; Munich, Germany), driven in remote mode by a Model 4053B signal generator (BK Precision, Yorba Linda California), was used to deliver stimulation instead. This equipment could not produce the slow ramps, so current was immediately switched on and off instead in these sessions. No significant differences between these sessions in terms of PLV change ($p > 0.31$; $Z=1.01$; Wilcoxon rank-sum test) or proportion of neurons affected ($p > 0.1$; $chi2 = 2.83$) was observed. Baseline and tACS blocks were separated by an intertrial interval of 1.5 or 5 minutes.

Although stimulation of peripheral afferents in the retina and skin can potentially confound behavioral experiments, we have previously demonstrated that neither likely account for the neural effects reported here (Vieira et al., 2020, Krause et al., 2019).

Electrophysiological Recording

The target structures were accessed through sterile plastic recording chambers implanted on the skull (Crist Instruments; Hagerstown, Maryland). After penetrating the dura with a 22-gauge

stainless steel guide tube, we lowered 32-channel linear arrays (V-Probe; Plexon: Dallas, Texas) into the target with a NAN Microdrive (NAN Instruments; Nazareth Illit, Israel). The location and depths of the targeted structures were confirmed via a post-operative CT (hippocampus) or MRI (V4).

The raw signals from each electrode were digitized by a Ripple Neural Interface Processsor (Ripple Neuro: Salt Lake City, Utah). During acquisition, the signals were band-pass filtered between 0.3 and 7500 Hz, digitized at 0.5µV/16-bit resolution, and stored at 30,000 Hz for subsequent analysis. The artifacts from tACS stimulation did not exceed the amplifier's linear range (±12 mV), allowing us to continuously record spiking and LFP signals during stimulation. Single units were identified offline by bandpass filtering the signal between 0.5 and 7 kHz with a third-order Butterworth filter. Spikes were initially detected as crossings exceeding a threshold of ±3 standard deviations, robustly estimated for each channel. Short segments around each threshold crossing were then extracted and clustered with UltraMegaSort 2000, a *k*-means based overclustering algorithm (Hill et al., 2011). Units were manually reviewed to ensure they had a consistent width and amplitude, a clear refractory period, and good separation in PCA space. Loss of signal during parts of the tACS cycle could produce spurious changes in entrainment, but control analyses for the same equipment and analysis pipeline suggest this is unlikely (e.g., Figure S2 of Krause et al., 2019).

Phase-locking analysis

We quantified neural entrainment by calculating pairwise phase consistency (PPC) values for each cell, a measure of the synchronization between the phase of an on-going signal (here, the LFP or tACS) and a point process (spiking activity). Although computationally intensive, this method has several statistical advantages over other common measures of phase-locking (Vinck et al., 2010).

These were calculated using spikes obtained from one channel and the continuous signal from an adjacent channel (150 µm away), so as to avoid spectral contamination that may artifactually inflate measures of entrainment (Zanos et al., 2011). Using this local signal, rather than measuring entrainment to copy of the tACS output, also ensures that referencing remained constant across conditions and accounts for any physiological distortion of the tACS waveform (Noury et al., 2016). To define the phase, the wideband signal was filtered into a ±1 Hz range around the frequency of interest (i.e., 4—6 or 19—21 Hz). The instantaneous phase at the time of each spike was derived from its Hilbert transform and used to calculate the PPC. PPCs were calculated for each condition separately and compared across conditions via a randomization test. For presentation purposes, these were then converted to phase-locking values (PLVs), a more commonly used measure of spike entrainment. Conveniently, PLVs are also equivalent (under some simplifying assumptions) to spike-field coherence, another oft-used metric of spike-LFP coupling. As we reviewed in Krause et al. (2019), the effect sizes reported here are similar to those produced by changes in behavioral state and sensory input, and therefore are likely to be physiologically relevant.

Quantification and Statistical Analysis

Where possible, statistical analyses were performed using nonparametric tests that avoid distributional assumptions; population-level analyses were carried using Wilcoxon rank-sum and sign-rank tests, as appropriate. We used 95 percent confidence intervals of the median as population dispersion, calculated using the formula in Campbell and Gardner (1988). All statistical tests are two-tailed, using sample sizes derived from our previous work. Significance of differences between categories was assessed using the chi-square test. Sample sizes were determined based on our previous work and data were analyzed using Matlab (The Mathworks, Natick, MA, USA), the CircStats toolbox (Berens, 2009), and Julia (Bezanson et al., 2017, Rackauckas and Nie, 2017).

Cell Type Identification

Labelling individual neurons from which data were collected is technically infeasible in non-human primates, so putative interneurons were identified based on the shape of their extracellular action potential. Many interneurons contain Kv3 potassium channels, whose fast deactivation rates help quickly repolarize the cell, causing the action potentials to become thinner than those produced by more sluggish channels present in excitatory cells (Rudy et al., 1999). The trough-to-peak width of the extracellular action potential has therefore been proposed as a method for separating putative inhibitory and excitatory cells (Mitchell et al., 2007). For each neuron, we measured the trough-to-peak width on its average waveform, using spikes collected in all conditions. Our data exhibited a clearly bimodal distribution (Figure 6A), and we applied a hard threshold at 250 µs (Vinck et al., 2013), classifying neurons with narrower spikes as putative interneurons and those with broader spikes as putative excitatory cells. Unsupervised clustering with a Gaussian mixture model yielded very similar classifications.

A more fine-grained categorization of cell types may be possible if additional features of the extracellular action potential are included in the clustering analysis (Trainito et al., 2019, Lee et al., 2021). However, it remains unclear how these functional categories map onto specific morphologies. On the other hand, the two-way classification used here allows us to test a specific hypothesis about the relationship between cell shape and determine if interneurons are less affected by exogenous electric fields.

However, not every narrow-spiking neuron in our data set is likely to be a fast-spiking GABAeric interneuron. Previous work has identified neurons that emit narrow action potentials despite having spiny, pyramidal morphology (Nowak et al., 2003, Haider et al., 2010) and, in primates, up to 25% of Kv3-expressing neurons are non-GABAergic (Constantinople et al., 2009). An alternate explanation for our findings in Figure 6 is that these non-GABAergic narrow-spiking neurons are affected by tACS, while the “true” interneurons are unresponsive. However, the proportion of affected cells in our data (23/51) is significantly higher than would be expected under a 25%/75% split ($p < 0.01$; $\chi(1) = 10.99$), suggesting that this is unlikely to occur in our data.

Model Simulations

The Stuart-Landau oscillator described above consists of two ordinary differential equations with 3 parameters (Doelling and Assaneo, 2021). The frequency of the ongoing oscillation is determined by the ω parameter, while its stability is controlled by λ: values above zero produce self-sustaining oscillations, while setting $\lambda < 0$ causes the oscillations to decay with time. Finally, γ dampens the system, controlling how quickly it settles into a steady-state amplitude.

The model equations were solved numerically using Matlab's `ode45` function, an explicit Runge-Kutta (4,5) method, using the solver's default parameters and the initial conditions $x = 0$, $y = -1$. The model was run for 200 s total. In stimulation conditions, the external drive *s(t)* was included only after 40 s so that the model could reach steady-state. In both cases, we defined the amplitude as $\sqrt{2}$ times root-mean-squared amplitude of the signal; this corresponds to an amplitude of 1 for a standard sine wave but corrects for any transients created by numerical integration. To generate Figure 4C, we evaluated all combinations of phase mismatch (0-315°, in steps of 45°) and frequency mismatch (50-150% of the baseline oscillation's cycle, in steps of 10%), for values of k ranging from 0 to 100% of the baseline oscillation's amplitude. These were then numerically integrated with Matlab's `trapz` to find the net effect across phase and frequency shown in Figure 4D. Similar results were obtained using Julia and its `Tsit5` solver.

As the model does not have explicit physical units, we performed a limited exploration of the parameter space, to determine whether a qualitative match to our data could be found. For Figure 4, the values were λ=0.2, ω=0.5, and λ=1.0, which were similar to those used in a previous study of the model (Doelling and Assaneo, 2021). However, these precise parameters were not required to reproduce the negative flanks shown in Figure 4C and 4D. We ran 250 additional simulations, setting λ, ω, and λ independently to values between 0.1 and 10; smaller values took prohibitively long to reach steady-state. In more than half of these simulations (162/250), at least one value of k (10-150%, in steps of 10%) reduced the total entrainment, as in Figure 4D. Indeed, the "quenching" behavior we have observed is actually a universal feature of many kinds of oscillators (Pikovsky et al., 2003), and as shown in the Supplemental Analysis, similar results can be derived analytically from a simplified version of this model.

References

ABERRA, A. S., PETERCHEV, A. V. & GRILL, W. M. 2018. Biophysically realistic neuron models for simulation of cortical stimulation. *J Neural Eng*, 15, 066023.

ALLEN, E. A., PASLEY, B. N., DUONG, T. & FREEMAN, R. D. 2007. Transcranial magnetic stimulation elicits coupled neural and hemodynamic consequences. *Science*, 317, 1918-21.

ANASTASSIOU, C. A., PERIN, R., MARKRAM, H. & KOCH, C. 2011. Ephaptic coupling of cortical neurons. *Nat Neurosci*, 14, 217-23.

BERENS, P. 2009. CircStat: A MATLAB Toolbox for Circular Statistics. *Journal of Statistical Software*, 31, 1 - 21.

BERENYI, A., BELLUSCIO, M., MAO, D. & BUZSAKI, G. 2012. Closed-loop control of epilepsy by transcranial electrical stimulation. *Science,* 337**,** 735-7.

BEZANSON, J., EDELMAN, A., KARPINSKI, S. & SHAH, V. B. 2017. Julia: A fresh approach to numerical computing. *SIAM review,* 59**,** 65-98.

BICHOT, N. P., ROSSI, A. F. & DESIMONE, R. 2005. Parallel and serial neural mechanisms for visual search in macaque area V4. *Science,* 308**,** 529-34.

BILKEY, D. K. & HEINEMANN, U. 1999. Intrinsic theta-frequency membrane potential oscillations in layer III/V perirhinal cortex neurons of the rat. *Hippocampus,* 9**,** 510-8.

BINDMAN, L. J., LIPPOLD, O. C. & REDFEARN, J. W. 1964. The Action of Brief Polarizing Currents on the Cerebral Cortex of the Rat (1) during Current Flow and (2) in the Production of Long-Lasting after-Effects. *J Physiol,* 172**,** 369-82.

BURNS, S. P., XING, D. & SHAPLEY, R. M. 2011. Is gamma-band activity in the local field potential of V1 cortex a "clock" or filtered noise? *J Neurosci,* 31**,** 9658-64.

CABRAL-CALDERIN, Y. & WILKE, M. 2020. Probing the Link Between Perception and Oscillations: Lessons from Transcranial Alternating Current Stimulation. *Neuroscientist,* 26**,** 57-73.

CAMPBELL, M. J. & GARDNER, M. J. 1988. Calculating confidence intervals for some non-parametric analyses. *Br Med J (Clin Res Ed),* 296**,** 1454-6.

CHALK, M., HERRERO, J. L., GIESELMANN, M. A., DELICATO, L. S., GOTTHARDT, S. & THIELE, A. 2010. Attention reduces stimulus-driven gamma frequency oscillations and spike field coherence in V1. *Neuron,* 66**,** 114-25.

CHAN, C. Y. & NICHOLSON, C. 1986. Modulation by applied electric fields of Purkinje and stellate cell activity in the isolated turtle cerebellum. *J Physiol,* 371**,** 89-114.

CHANDER, B. S., WITKOWSKI, M., BRAUN, C., ROBINSON, S. E., BORN, J., COHEN, L. G., BIRBAUMER, N. & SOEKADAR, S. R. 2016. tACS Phase Locking of Frontal Midline Theta Oscillations Disrupts Working Memory Performance. *Front Cell Neurosci,* 10**,** 120.

CHIANG, A. K., RENNIE, C. J., ROBINSON, P. A., VAN ALBADA, S. J. & KERR, C. C. 2011. Age trends and sex differences of alpha rhythms including split alpha peaks. *Clin Neurophysiol,* 122**,** 1505-17.

COHEN, M. R. & MAUNSELL, J. H. 2009. Attention improves performance primarily by reducing interneuronal correlations. *Nat Neurosci,* 12**,** 1594-600.

COLE, S. R. & VOYTEK, B. 2017. Brain Oscillations and the Importance of Waveform Shape. *Trends Cogn Sci,* 21**,** 137-149.

CONSTANTINOPLE, C. M., DISNEY, A. A., MAFFIE, J., RUDY, B. & HAWKEN, M. J. 2009. Quantitative analysis of neurons with Kv3 potassium channel subunits, Kv3.1b and Kv3.2, in macaque primary visual cortex. *J Comp Neurol,* 516**,** 291-311.

DATTA, A., KRAUSE, M.R., PILLY, P.K., CHOE, J., ZANOS, T.P., THOMAS, C., AND PACK, C.C. 2016. On comparing in vivo intracranial recordings in non-human primates to predictions of optimized transcranial electrical stimulation. *Proceedings of the 38th Annual International Conference of the IEEE Engineering in Medicine and Biology Society*.

DEANS, J. K., POWELL, A. D. & JEFFERYS, J. G. 2007. Sensitivity of coherent oscillations in rat hippocampus to AC electric fields. *J Physiol,* 583**,** 555-65.

DOELLING, K. B. & ASSANEO, M. F. 2021. Neural oscillations are a start toward understanding brain activity rather than the end. *PLoS Biol,* 19**,** e3001234.

EHRHARDT, S. E., FILMER, H. L., WARDS, Y., MATTINGLEY, J. B. & DUX, P. E. 2021. The influence of tDCS intensity on decision-making training and transfer outcomes. *J Neurophysiol,* 125**,** 385-397.

FEURRA, M., PASQUALETTI, P., BIANCO, G., SANTARNECCHI, E., ROSSI, A. & ROSSI, S. 2013. State-dependent effects of transcranial oscillatory currents on the motor system: what you think matters. *J Neurosci,* 33**,** 17483-9.

FRIES, P. 2015. Rhythms for Cognition: Communication through Coherence. *Neuron,* 88**,** 220-35.

FRIES, P., REYNOLDS, J. H., RORIE, A. E. & DESIMONE, R. 2001. Modulation of oscillatory neuronal synchronization by selective visual attention. *Science,* 291**,** 1560-3.

FROHLICH, F. & MCCORMICK, D. A. 2010. Endogenous electric fields may guide neocortical network activity. *Neuron,* 67**,** 129-43.

GROVER, S., NGUYEN, J. A. & REINHART, R. M. G. 2021. Synchronizing Brain Rhythms to Improve Cognition. *Annu Rev Med,* 72**,** 29-43.

GUAN, Y., GUPTA, V., KASHINATH, K. & LI, L. K. B. 2019. Open-loop control of periodic thermoacoustic oscillations: Experiments and low-order modelling in a synchronization framework. *Proceedings of the Combustion Institute,* 37**,** 5315-5323.

GUNDLACH, C., MULLER, M. M., NIERHAUS, T., VILLRINGER, A. & SEHM, B. 2016. Phasic Modulation of Human Somatosensory Perception by Transcranially Applied Oscillating Currents. *Brain Stimul,* 9**,** 712-719.

HAIDER, B., KRAUSE, M. R., DUQUE, A., YU, Y., TOURYAN, J., MAZER, J. A. & MCCORMICK, D. A. 2010. Synaptic and network mechanisms of sparse and reliable visual cortical activity during nonclassical receptive field stimulation. *Neuron,* 65**,** 107-21.

HELFRICH, R. F., SCHNEIDER, T. R., RACH, S., TRAUTMANN-LENGSFELD, S. A., ENGEL, A. K. & HERRMANN, C. S. 2014. Entrainment of brain oscillations by transcranial alternating current stimulation. *Curr Biol,* 24**,** 333-9.

HERRMANN, C. S., MURRAY, M. M., IONTA, S., HUTT, A. & LEFEBVRE, J. 2016. Shaping Intrinsic Neural Oscillations with Periodic Stimulation. *J Neurosci,* 36**,** 5328-37.

HILL, D. N., MEHTA, S. B. & KLEINFELD, D. 2011. Quality metrics to accompany spike sorting of extracellular signals. *J Neurosci,* 31**,** 8699-705.

HOLT, A. B., KORMANN, E., GULBERTI, A., POTTER-NERGER, M., MCNAMARA, C. G., CAGNAN, H., BAASKE, M. K., LITTLE, S., KOPPEN, J. A., BUHMANN, C., WESTPHAL, M., GERLOFF, C., ENGEL, A. K., BROWN, P., HAMEL, W., MOLL, C. K. E. & SHAROTT, A. 2019. Phase-Dependent Suppression of Beta Oscillations in Parkinson's Disease Patients. *J Neurosci,* 39**,** 1119-1134.

HUANG, W. A., STITT, I. M., NEGAHBANI, E., PASSEY, D. J., AHN, S., DAVEY, M., DANNHAUER, M., DOAN, T. T., HOOVER, A. C., PETERCHEV, A. V., RADTKE-SCHULLER, S. & FROHLICH, F. 2021. Transcranial alternating current stimulation entrains alpha oscillations by preferential phase synchronization of fast-spiking cortical neurons to stimulation waveform. *Nat Commun,* 12**,** 3151.

HUANG, Y., LIU, A. A., LAFON, B., FRIEDMAN, D., DAYAN, M., WANG, X., BIKSON, M., DOYLE, W. K., DEVINSKY, O. & PARRA, L. C. 2017. Measurements and models of electric fields in the in vivo human brain during transcranial electric stimulation. *Elife,* 6.

JACKSON, M. P., RAHMAN, A., LAFON, B., KRONBERG, G., LING, D., PARRA, L. C. & BIKSON, M. 2016. Animal models of transcranial direct current stimulation: Methods and mechanisms. *Clin Neurophysiol,* 127**,** 3425-3454.

JENSEN, O., GELFAND, J., KOUNIOS, J. & LISMAN, J. E. 2002. Oscillations in the alpha band (9-12 Hz) increase with memory load during retention in a short-term memory task. *Cereb Cortex,* 12**,** 877-82.

JOHNSON, L., ALEKSEICHUK, I., KRIEG, J., DOYLE, A., YU, Y., VITEK, J., JOHNSON, M. & OPITZ, A. 2020. Dose-dependent effects of transcranial alternating current stimulation on spike timing in awake nonhuman primates. *Sci Adv,* 6.

KAR, K., DUIJNHOUWER, J. & KREKELBERG, B. 2017. Transcranial Alternating Current Stimulation Attenuates Neuronal Adaptation. *J Neurosci,* 37**,** 2325-2335.

KASTEN, F. H., DUECKER, K., MAACK, M. C., MEISER, A. & HERRMANN, C. S. 2019. Integrating electric field modeling and neuroimaging to explain inter-individual variability of tACS effects. *Nat Commun,* 10**,** 5427.

KETZ, N., JONES, A. P., BRYANT, N. B., CLARK, V. P. & PILLY, P. K. 2018. Closed-Loop Slow-Wave tACS Improves Sleep-Dependent Long-Term Memory Generalization by Modulating Endogenous Oscillations. *J Neurosci,* 38**,** 7314-7326.

KLIMESCH, W. 2012. alpha-band oscillations, attention, and controlled access to stored information. *Trends Cogn Sci,* 16**,** 606-17.

KRAUSE, M. R., VIEIRA, P. G., CSORBA, B. A., PILLY, P. K. & PACK, C. C. 2019. Transcranial alternating current stimulation entrains single-neuron activity in the primate brain. *Proc Natl Acad Sci U S A,* 116**,** 5747-5755.

LEE, E. K., BALASUBRAMANIAN, H., TSOLIAS, A., ANAKWE, S. U., MEDALLA, M., SHENOY, K. V. & CHANDRASEKARAN, C. 2021. Non-linear dimensionality reduction on extracellular waveforms reveals cell type diversity in premotor cortex. *Elife,* 10.

LIU, A., VOROSLAKOS, M., KRONBERG, G., HENIN, S., KRAUSE, M. R., HUANG, Y., OPITZ, A., MEHTA, A., PACK, C. C., KREKELBERG, B., BERENYI, A., PARRA, L. C., MELLONI, L., DEVINSKY, O. & BUZSAKI, G. 2018. Immediate neurophysiological effects of transcranial electrical stimulation. *Nat Commun,* 9**,** 5092.

LIU, L. D., HAEFNER, R. M. & PACK, C. C. 2016. A neural basis for the spatial suppression of visual motion perception. *Elife,* 5.

MANSOURI, F., DUNLOP, K., GIACOBBE, P., DOWNAR, J. & ZARIFFA, J. 2017. A Fast EEG Forecasting Algorithm for Phase-Locked Transcranial Electrical Stimulation of the Human Brain. *Front Neurosci,* 11**,** 401.

MARCHESOTTI, S., NICOLLE, J., MERLET, I., ARNAL, L. H., DONOGHUE, J. P. & GIRAUD, A. L. 2020. Selective enhancement of low-gamma activity by tACS improves phonemic processing and reading accuracy in dyslexia. *PLoS Biol,* 18**,** e3000833.

MATHEWSON, K. J., JETHA, M. K., DRMIC, I. E., BRYSON, S. E., GOLDBERG, J. O. & SCHMIDT, L. A. 2012. Regional EEG alpha power, coherence, and behavioral symptomatology in autism spectrum disorder. *Clin Neurophysiol,* 123**,** 1798-809.

MITCHELL, J. F., SUNDBERG, K. A. & REYNOLDS, J. H. 2007. Differential attention-dependent response modulation across cell classes in macaque visual area V4. *Neuron,* 55**,** 131-41.

MOGUL, D. J. & VAN DRONGELEN, W. 2014. Electrical control of epilepsy. *Annu Rev Biomed Eng,* 16**,** 483-504.

MORI, H. & KURAMOTO, Y. 1998. *Dissipative Structures and Chaos,* Tokyo, Iwanami Shoten, Publishers.

NOURY, N., HIPP, J. F. & SIEGEL, M. 2016. Physiological processes non-linearly affect electrophysiological recordings during transcranial electric stimulation. *Neuroimage,* 140**,** 99-109.

NOWAK, L. G., AZOUZ, R., SANCHEZ-VIVES, M. V., GRAY, C. M. & MCCORMICK, D. A. 2003. Electrophysiological classes of cat primary visual cortical neurons in vivo as revealed by quantitative analyses. *J Neurophysiol,* 89**,** 1541-66.

OKUHATA, S., KUSANAGI, T. & KOBAYASHI, T. 2013. Parietal EEG alpha suppression time of memory retrieval reflects memory load while the alpha power of memory maintenance is a composite of the visual process according to simultaneous and successive Sternberg memory tasks. *Neurosci Lett,* 555**,** 79-84.

OLDHAM, P. D. 1962. A note on the analysis of repeated measurements of the same subjects. *J Chronic Dis,* 15**,** 969-77.

OZEN, S., SIROTA, A., BELLUSCIO, M. A., ANASTASSIOU, C. A., STARK, E., KOCH, C. & BUZSAKI, G. 2010. Transcranial electric stimulation entrains cortical neuronal populations in rats. *J Neurosci,* 30**,** 11476-85.

PARK, E. H., BARRETO, E., GLUCKMAN, B. J., SCHIFF, S. J. & SO, P. 2005. A model of the effects of applied electric fields on neuronal synchronization. *J Comput Neurosci,* 19**,** 53-70.

PASLEY, B. N., ALLEN, E. A. & FREEMAN, R. D. 2009. State-dependent variability of neuronal responses to transcranial magnetic stimulation of the visual cortex. *Neuron,* 62**,** 291-303.

PIKOVSKY, A., KURTHS, J., ROSENBLUM, M. & KURTHS, J. 2003. *Synchronization: a universal concept in nonlinear sciences*, Cambridge university press.

PREMRAJ, D., MANOJ, K., PAWAR, S. A. & SUJITH, R. I. 2021. Effect of amplitude and frequency of limit cycle oscillators on their coupled and forced dynamics. *Nonlinear Dynamics,* 103**,** 1439-1452.

RACKAUCKAS, C. & NIE, Q. 2017. DifferentialEquations.jl – A Performant and Feature-Rich Ecosystem for Solving Differential Equations in Julia. *Journal of Open Research Software,* 5.

RADMAN, T., RAMOS, R. L., BRUMBERG, J. C. & BIKSON, M. 2009. Role of cortical cell type and morphology in subthreshold and suprathreshold uniform electric field stimulation in vitro. *Brain Stimul,* 2**,** 215-28, 228 e1-3.

REATO, D., RAHMAN, A., BIKSON, M. & PARRA, L. C. 2010. Low-intensity electrical stimulation affects network dynamics by modulating population rate and spike timing. *J Neurosci,* 30**,** 15067-79.

REATO, D., RAHMAN, A., BIKSON, M. & PARRA, L. C. 2013. Effects of weak transcranial alternating current stimulation on brain activity-a review of known mechanisms from animal studies. *Front Hum Neurosci,* 7**,** 687.

RUDY, B., CHOW, A., LAU, D., AMARILLO, Y., OZAITA, A., SAGANICH, M., MORENO, H., NADAL, M. S., HERNANDEZ-PINEDA, R., HERNANDEZ-CRUZ, A., ERISIR, A., LEONARD, C. & VEGA-SAENZ DE MIERA, E. 1999. Contributions of Kv3 channels to neuronal excitability. *Ann N Y Acad Sci,* 868**,** 304-43.

SANTANIELLO, S., MCCARTHY, M. M., MONTGOMERY, E. B., JR., GALE, J. T., KOPELL, N. & SARMA, S. V. 2015. Therapeutic mechanisms of high-frequency

stimulation in Parkinson's disease and neural restoration via loop-based reinforcement. *Proc Natl Acad Sci U S A,* 112**,** E586-95.
SCHAEFER, A. T., ANGELO, K., SPORS, H. & MARGRIE, T. W. 2006. Neuronal oscillations enhance stimulus discrimination by ensuring action potential precision. *PLoS Biol,* 4**,** e163.
SHIRHATTI, V., BORTHAKUR, A. & RAY, S. 2016. Effect of Reference Scheme on Power and Phase of the Local Field Potential. *Neural Comput,* 28**,** 882-913.
SOFTKY, W. R. & KOCH, C. 1993. The highly irregular firing of cortical cells is inconsistent with temporal integration of random EPSPs. *J Neurosci,* 13**,** 334-50.
SPYROPOULOS, G., BOSMAN, C. A. & FRIES, P. 2018. A theta rhythm in macaque visual cortex and its attentional modulation. *Proc Natl Acad Sci U S A,* 115**,** E5614-E5623.
TRAINITO, C., VON NICOLAI, C., MILLER, E. K. & SIEGEL, M. 2019. Extracellular Spike Waveform Dissociates Four Functionally Distinct Cell Classes in Primate Cortex. *Curr Biol,* 29**,** 2973-2982 e5.
VENABLES, N. C., BERNAT, E. M. & SPONHEIM, S. R. 2009. Genetic and disorder-specific aspects of resting state EEG abnormalities in schizophrenia. *Schizophr Bull,* 35**,** 826-39.
VIEIRA, P. G., KRAUSE, M. R. & PACK, C. C. 2020. tACS entrains neural activity while somatosensory input is blocked. *PLoS Biol,* 18**,** e3000834.
VINCK, M., VAN WINGERDEN, M., WOMELSDORF, T., FRIES, P. & PENNARTZ, C. M. 2010. The pairwise phase consistency: a bias-free measure of rhythmic neuronal synchronization. *Neuroimage,* 51**,** 112-22.
VINCK, M., WOMELSDORF, T., BUFFALO, E. A., DESIMONE, R. & FRIES, P. 2013. Attentional modulation of cell-class-specific gamma-band synchronization in awake monkey area v4. *Neuron,* 80**,** 1077-89.
VOROSLAKOS, M., TAKEUCHI, Y., BRINYICZKI, K., ZOMBORI, T., OLIVA, A., FERNANDEZ-RUIZ, A., KOZAK, G., KINCSES, Z. T., IVANYI, B., BUZSAKI, G. & BERENYI, A. 2018. Direct effects of transcranial electric stimulation on brain circuits in rats and humans. *Nat Commun,* 9**,** 483.
WATERSTON, M. L. & PACK, C. C. 2010. Improved discrimination of visual stimuli following repetitive transcranial magnetic stimulation. *PLoS One,* 5**,** e10354.
WILSCH, A., NEULING, T., OBLESER, J. & HERRMANN, C. S. 2018. Transcranial alternating current stimulation with speech envelopes modulates speech comprehension. *Neuroimage,* 172**,** 766-774.
ZANOS, T. P., MINEAULT, P. J., GUITTON, D. & PACK, C. C. 2016. Mechanisms of Saccadic Suppression in Primate Cortical Area V4. *J Neurosci,* 36**,** 9227-39.
ZANOS, T. P., MINEAULT, P. J., NASIOTIS, K. T., GUITTON, D. & PACK, C. C. 2015. A sensorimotor role for traveling waves in primate visual cortex. *Neuron,* 85**,** 615-27.
ZANOS, T. P., MINEAULT, P. J. & PACK, C. C. 2011. Removal of spurious correlations between spikes and local field potentials. *J Neurophysiol,* 105**,** 474-86.
ZOHARY, E., CELEBRINI, S., BRITTEN, K. H. & NEWSOME, W. T. 1994. Neuronal plasticity that underlies improvement in perceptual performance. *Science,* 263**,** 1289-92.

SI Figures

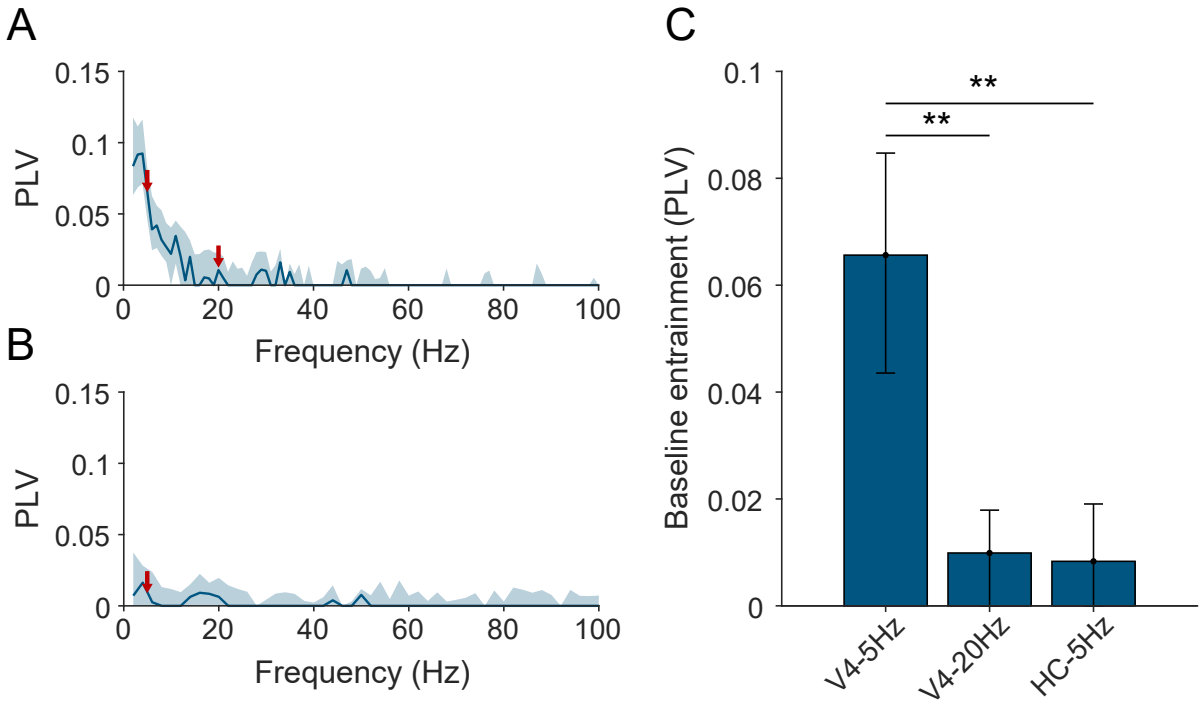

Figure S1. Baseline entrainment of neurons in each experimental condition. A) Entrainment spectra for V4 neurons (N=157), showing phase-locking to the local field potential in ± 1 Hz frequency bands. The median and 95% confidence interval are shown, calculated from all V4 neurons (i.e., those used in subsequent 5 Hz and 20 Hz tACS experiments). Red arrows indicate the tACS frequencies used in those experiments. **B)** Entrainment spectra for hippocampal neurons (N=21), plotted in the same style. C) Population summary, showing the median and 95% confidence interval for baseline entrainment across the experimental conditions. ** indicates $p < 0.01$. See also Main Figure 1 for individual data points; note that the V4 data is divided across Panels A and B of Main Figure 1.

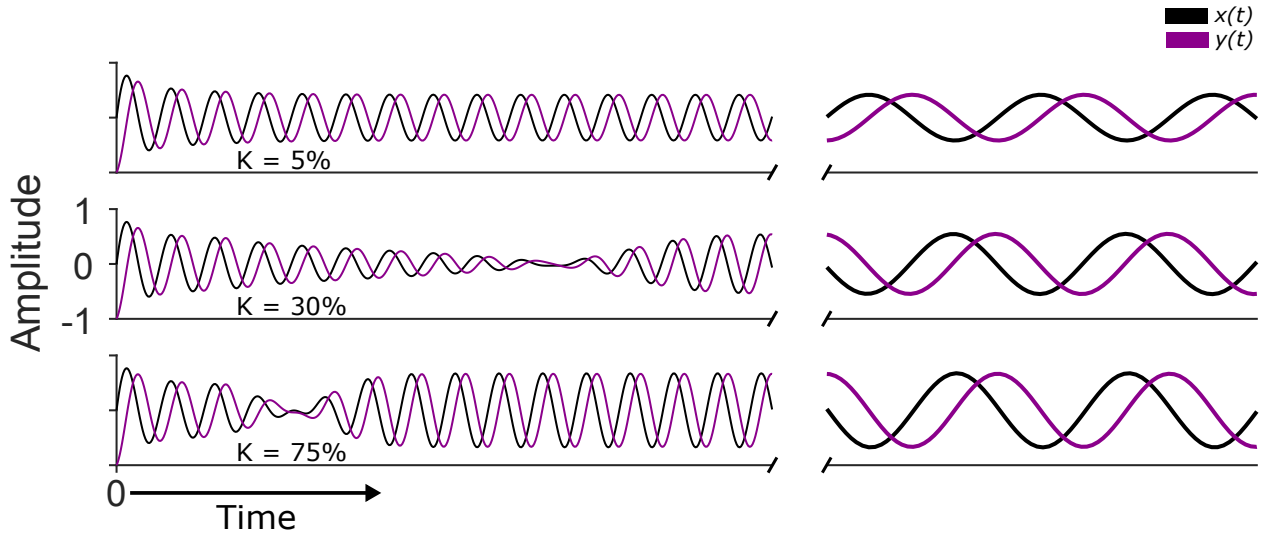

Figure S2. Both model populations are affected similarly by tACS. The values of *x* (black) and *y* (magenta) during three runs of the model with *k* = 5, 30, and 75 percent, demonstrating that they are phase-shifted copies of each other. Note that baseline is not shown here. See also Main Figure 4.

SI Analysis

Asynchronous Quenching in Simplified Stuart-Landau Oscillators

We start with a system of two coupled Stuart-Landau oscillators

$$\frac{dx}{dt} = \lambda x - 2\pi\omega y - \gamma\left(x^2 + y^2\right)x + s(t)$$
$$\frac{dy}{dt} = \lambda y + 2\pi\omega x - \gamma\left(x^2 + y^2\right)y$$

where *s(t)* is a periodic forcing of the form $s(t) = k\,\sin(2\pi\omega_s t + \phi_s)$, where *k* is its amplitude and ω_s is the frequency of the stimulation. The central result of the model presented in the paper (Figure 4) is that of "asynchronous quenching": entrainment is maximal when the frequency of the forcing ω_s is closest to the intrinsic frequency of the oscillators ω. This result cannot be explained by a simple summation of periodic oscillations corresponding to the intrinsic and driven waves, regardless of their phase offset. . To gain a mechanistic understanding of this finding, it is worthwhile to consider a simplified linear system obtained by setting $\gamma = 0$, which reduces the model to

$$\frac{dx}{dt} = \lambda x - 2\pi\omega y + s(t)$$
$$\frac{dy}{dt} = \lambda y + 2\pi\omega x$$

When $k = 0$, the eigenvalues of the above expressions are $\lambda \pm i\omega$, so setting $\lambda < 0$ ensures that the system is globally stable. Its dynamics are therefore easy to track analytically, but the behavior of the model is simplified: there are no reductions in entrainment as in Figure 4C and 4D. We can derive the maximal amplitude of the forced oscillator in this simplified expression (Mori and Kuramoto, 1998):

$$\hat{x} \approx \frac{k\sqrt{2\pi\omega}}{\sqrt{\left(2\pi\omega\right)^2\Delta_\omega + (2\pi\omega)^2}}$$

where $\Delta_\omega = \left(2\pi\omega - 2\pi\omega_s\right)^2$. Here, the numerator reflects the amplitude and frequency of the forced oscillation, while the denominator takes into account the difference between the intrinsic and forced oscillation's frequencies. As an example, consider numerical simulation where a 2Hz forced oscillation is applied that matched the intrinsic frequency (i.e., $\omega = \omega_s = 2$ Hz and therefore $\Delta_w = 0$). In this case, the response of *x* is prominent (Figure S3, top row). However, with unmatched frequencies ($\omega_s = 1$ Hz or $\omega_s = 3$ Hz), the response is attenuated. Interestingly, similar results are obtained even when the intrinsic oscillation is left to vanish before the forced oscillation is applied (Figure S3, bottom row). With $\lambda = -1$, Figure S4A shows agreement between the numerical and analytical results. This is robust against changes in phase, which alters the shape of the response without compromising the fit obtained from $\hat{x}$, as shown in Figure S4B. Finally, a similar distribution is obtained with $\lambda = 0.1$, though in this case the system's eigenvalues are positive and therefore the amplitude of *x* is markedly higher

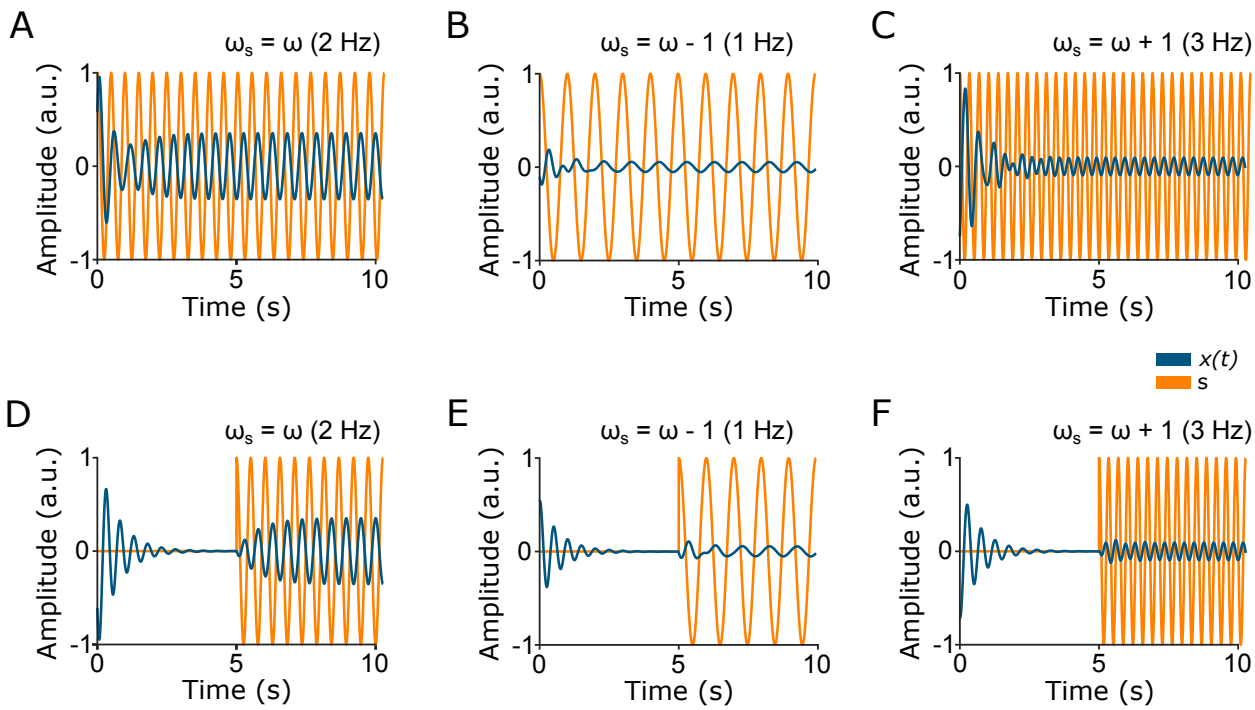

Figure S3. Driving a Stuart-Landau system with a forced oscillation. In all panels, ω was set to 2 Hz while the frequency of stimulation ω_s was varied. **A-C)** Stimulation (orange line) was applied to an ongoing oscillation (blue) at the same frequency (A), at a slightly lower frequency (B), and at a slightly higher frequency (C). **D-F)** As above, except that the ongoing oscillation was allowed to decay before stimulation was applied

(Figure S4C) and not amenable to the approximation described above. In all cases shown in Figure S4, the range of forced frequencies leading to a change in the mean amplitude of *x* depends on *k*, with larger values broadening this range.

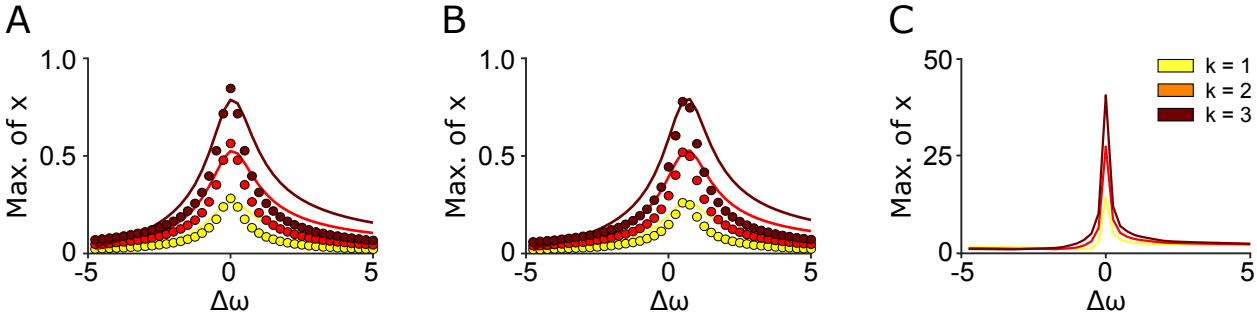

Figure S4. Comparison of numerical and analytical results. **A-B)** Filled circles indicate the analytical solution $\hat{x}$, while the lines are derived from the numerical simulation. In all panels the intrinsic frequency was set to 5 Hz with a phase shift of the forced oscillation set to zero (A) or 1.5 radians (B). **C)** Similar results were obtained from an unstable model where $\lambda = 0.1$.

Finally, asynchronous quenching can also be obtained in coupled oscillators where a time delay is introduced, as shown in Figure S5.

$$\frac{dx}{dt} = (\lambda - d)x(t) - 2\pi\omega y(t-d) + s(t)$$
$$\frac{dy}{dt} = (\lambda - d)y(t) + 2\pi\omega x(t-d)$$

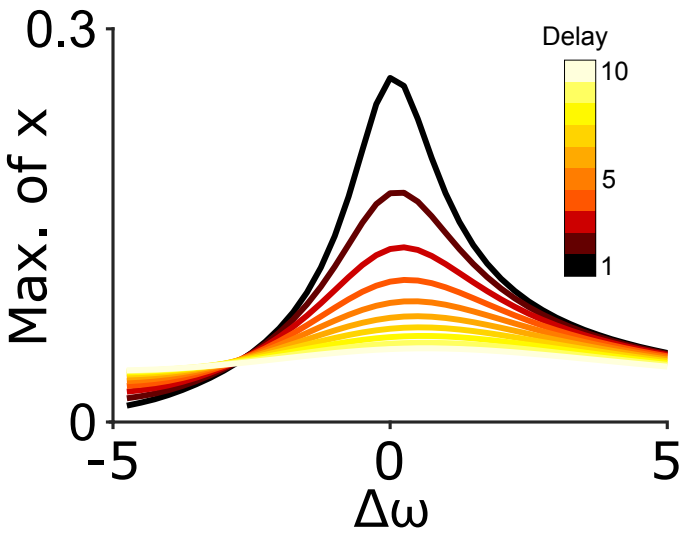

Figure S5. Asynchronous quenching is robust to delays between the two oscillators. Results of simulations where the delays ranged from 1 (black) to 10 (yellow).